

Dynamic identification and static loading tests of timber vaults. Application to a Modernist 20th century heritage structure

Yohei Endo^{*1}, Miquel Llorens², Pere Roca³, Luca Pelà⁴

¹ Shinshu University, Department of Architecture, Wakasato 4-17-1, 380-8553, Nagano, Japan

² University of Girona, Department of Mechanical Engineering and Industrial Construction, C/ M. Aurèlia Campmany, 63 17003 Girona, Spain

³ Universitat Politècnica de Catalunya (UPC-BarcelonaTech), Department of Civil and Environmental Engineering, Jordi Girona 1-3, 08034 Barcelona, Spain

**corresponding author, e-mail: endii@shinshu-u.ac.jp, phone: +81 26 269 5345, fax +81 26 269 5364*

ABSTRACT

This paper presents the study of the structural performance of a set of timbrel vaults belonging to the so-called Administration Pavilion of the Hospital de Sant Pau, a large-scale hospital complex located in Barcelona. The paper includes three parts. First, the Administration pavilion of Hospital de Sant Pau is described by putting the emphasis on the geometry of the masonry vaults and the combined utilisation of steel and masonry structural members. Second, laboratory and in-situ experiments are discussed. Finally, the behaviour observed during the dynamic-identification and the static-loading tests is simulated by means of FEM analysis. The FEM models prepared to analyse the vaults take explicitly into account the direct effect of secondary masonry structural elements, such as the upper slab and the extrados stiffening diaphragms. The comparison indicates that the consideration of these structural elements is essential for an adequate FEM simulation of both the dynamic and the static behaviour of the timbrel vaults.

KEYWORDS: brick masonry, timbrel vault, extrados stiffening diaphragm, dynamic identification test, static loading test, FEM analysis.

1 INTRODUCTION

Timbrel vaulting (also known as Catalan vaulting) is a masonry construction technique perfected in Catalonia, Spain, and widely employed during the 19th and the beginning of the 20th century. Today the word “timbrel vault” denotes a curvilinear element composed of up to four layers of tiles. The tiles, generally with dimensions around 150 × 300 × 15 mm³, were bonded together with gypsum and lime mortar. The lower layer was built with gypsum mortar in order to allow a quick hardening, thus making unnecessary the use of a centering. The upper layers were built with lime mortar in earlier times and or even adding Portland cement mortar in later times (Truñó, 2004). The origin of timbrel vaulting is not known (Collins, 1968) but the first document on this construction technique may date back to 1382 (Araguas, 1999). Timbrel vaults are characterised by high loading capacity compared to their reduced thickness (Moya, 1947).

The construction and the strength performance of timber vaults were discussed by different authors (Gulli and Mochi, 1995, González, 1999, González, 2005, Huerta et al., 2001). A comprehensive review of the history of timber vaults was presented by Huerta (2003). The 19th century experiments carried out on a timber vault, in France, were discussed by Redondo (2012). However, it is worth mentioning that very few research contributions are available about the characterisation of the structural behaviour and strength of timber vaults.

One of the earliest documents that made mention of structural design of timber vaults is “*Arte y Uso de Arquitectura*”, written by Fray Lorenzo de San Nicolás in 1639 (Fray Lorenzo, 1796). Fray Lorenzo built several timber vaults during the 17th century. He introduced general rules for the design of the depth of the buttresses as a ratio of the span of different types of vaults. According to Fray Lorenzo, the buttress of a timber vault could have a lesser depth ($1/5$ of the span) than other types of stone or brick vaults ($1/3$ and $1/4$ of the span). In the 18th century, D’Espie, a French nobleman, stated that timber vaults were solid enough to avoid cracks when they were built with good-quality mortar (D’Espie, 1754). Rafael Guastavino, a Spanish architect, brought the Catalan-vaulting technique to the United States at the end of the 19th century. He refined the construction technique and built various monumental buildings with the so-called Guastavino vaulting technique between 1890 and 1900 in the eastern United States. He also carried out a study on the structural behaviour of the timber vault structural system (Guastavino, 1893). According to him, and in contrast with conventional one-layer arched structural systems, structural stability of a timber vault was based on the cohesion of materials. Cohesive-force action appeared due to the mortar existing along the units.

Timber vaults can exhibit cracks and hinges very similar to those of other types of masonry vaults (Huerta, 2003). However, timber vaults can be constructed with light provisional supports or even without centering due to their cohesiveness. For the same reason, masons can walk

over the vault right after the construction. Therefore, a remarkable advantage of timber vaults can be seen in the construction process compared to other types of vaults.

Recently, Palizzolo et al. (2008) presented laboratory and in-situ static loading tests carried out on an existing timber vaulted building. De Llorens (2013) presented a study on 20th-century wineries composed of timber vaults. Ferrario et al. (2012) analysed a thin single-leaf vault and evaluated its seismic vulnerability through cyclic loading tests. A recent interesting project that drew inspiration from the traditional timber vaulting systems can be found in López et al. (2014).

The objective of the paper is to study the dynamic and static behaviour of complex timber masonry vaults through the execution of experimental tests and their subsequent simulations by means of the FE analysis. The research analyses the behaviour of the existing timber vaults of an outstanding modernist 20th century heritage structure, the Hospital de Sant Pau in Barcelona, Spain. The paper includes three parts. First, the structure of the Administration pavilion of Hospital de Sant Pau is presented with focus on the geometry of the vaults and the particular combination of steel and masonry members. Second, laboratory and in-situ experiments conducted on this building are described. The experiments included laboratory mechanical tests on brick and masonry along with in-situ static loading tests and dynamic identification tests. Finally, a comparison is made between the results from the dynamic identification and static loading tests and the corresponding predictions yield by on-purpose developed FEM models. These analyses pay particular attention to the role of the secondary structural elements that compose the vault, such as the upper masonry slab and the extrados diaphragms supporting the slab. The masonry diaphragms, also called ribs (or “frenelli” in Italy, where they can be frequently found in existing vaulted systems), are transverse vertical elements built at the extrados of the vaults as stiffening elements. The developed FEM models take into account the frictional behaviour of the masonry-to-masonry contacts between the stiffening diaphragms, the upper slab and the vault. Given the limited knowledge of the explicit role of upper slabs and stiffening diaphragms in the response of timber vaults, the novel character of the paper mainly

relies on the careful investigation of their behaviour by combined experimental and numerical approaches.

2 DESCRIPTION OF THE BUILDING

2.1 Note on the history of Hospital Sant Pau

The design of a large hospital was assigned to the architect Lluís Domènech i Montaner in 1901. This complex is today known as Hospital de la Santa Creu i de Sant Pau and is located in Barcelona, Spain (Figure 1). Part of the complex was designed and built until 1913. Domènech i Montaner designed the buildings by basing strongly on two modern concepts relevant to the architectural hygiene of hospitals. Firstly, patients were supposed to breathe pure air, as it improved recovery rates and decreased mortality. Secondly, it was important to group the patients according to the type of illness. Domènech i Montaner achieved the former concept by creating sufficient volume and by providing effective ventilation to the buildings. The latter was realised by designing the hospital as a set of different individual pavilions. Today the Hospital de Sant Pau is considered one of the major examples of the Catalan Modernism that prospered in Barcelona at the beginning of the 20th century. The historical part of the complex was included to the UNESCO World Heritage List in 1997.

Till recently, the complex was used as a hospital. However, since there was the need of additional space and more modern facilities, the construction of a new hospital complex started in 1990. The construction of the new hospital in a different site led to the need for the restoration of the modernist buildings and their adaptation to new uses. Most of the buildings are currently intended to accommodate offices for international organisations. Along with the restoration of the modernist pavilions, comprehensive studies were conducted from the architectural and structural point of view. These studies fostered respectful conservation and rehabilitation interventions. In most of the pavilions, valueless additions built during the mid-late 20th century, such as intermediate floor slabs and partition walls, were dismantled in order to recover the

original spaces and structures conceived by Domènech i Muntaner. More information about the history of the Hospital de Sant Pau is presented by González et al. (2011).

2.2 Description of the Administration pavilion

The structure of the building analysed, namely the Administration pavilion, is discussed in this section. More information on the structure of some of the pavilions of the Hospital complex can be found in other works (González, 2005, González et al., 2011, Casals et al., 2011).

This Administration pavilion is situated at the entrance of the Hospital de Sant Pau (Figure 1). It is the biggest building and its prominent appearance gives the visitors a splendid impression of the complex (Figures 2a,b). The building is symmetric in plan (Figure 2c). It is composed of five parts: a central body (corresponding to zone 1 in Figure 2c), the east and west middle bodies (corresponding to zones 2, 4) and the east and west extreme bodies (corresponding to zones 3, 5). This is a four-storey building composed of basement, ground floor and two upper floors. Masonry is composed of clay bricks and lime mortar in both vaults and walls. The building contains 130 timbrel vaults. The vaults' intrados is decorated with vitrified tiles (Figure 2b). In the Administration pavilion, most of the steel profiles are only located horizontally and are used to retain the thrust of the vaults, while, unlike the other pavilions, the vaults are supported on masonry load-bearing walls (Figure 2d). In the other buildings, for instance in eight almost identical pavilions located behind the Administration pavilion (Figure 1), the steel profiles are installed inside the walls and arches and at bottoms of the vaults. These steel members were considered to absorb the normal and bending forces caused by the arches and vaults.

In this paper, three double-curvature vaults are studied, herein identified as vaults A (the vault with shorter dimensions), B (selected vault with intermediate dimensions) and C (vault with longest dimensions). These vaults are shown in Figure 2e and described in the following paragraphs.

Vault A is located on the basement floor of the west middle body (zone 4) (Figure 2c, e). Six vaults of the same dimension are located in a row (Figure 3a). The space covered by the six vaults is used as a corridor giving access to larger rooms, including the room roofed by vault B (Figure 2e). The dimensions of the vault are $3.12 \times 3.12 \text{ m}^2$ in plan. The thickness of the vault is 0.12 m. The rise at the perimeters of the vault is 0.6 m. The vault is supported on a 4.6 m high and 0.35 m deep walls. There are two steel profiles IPN 80 located along the longitudinal perimeter of the vault's upper slab (Figure 2e).

Vault B is located in the basement floor of the West middle body (zone 4) (Figure 2c, e, Figure 3b). There are two vaults of the same dimensions in this floor. The dimensions of the vault in plan are $6.7 \times 6.2 \text{ m}^2$. The thickness of the vault is 0.12 m. The rise at the perimeters of the vault is 0.11 m. The vault is supported on 3.9 m high and 0.35 m deep walls. As in the previous case, there are two horizontal steel profiles IPN 80 placed along the perimeter of the vault's upper slab.

Vault C is located in the room of the basement floor of the West extreme body (zone 5) (Figure 2c, e). There are two vaults of the same dimensions separated by a masonry arch in the room (Figure 3c). The dimensions of the vault are $8.8 \times 8.8 \text{ m}^2$ in plan. The thickness of the vault is 0.08 m. The rise at the centre of the vault is 0.13 m. The supporting walls have a height of 4.3 m and a thickness of 0.76 m (Figure 3c). Two steel profiles IPN 100 are placed horizontally along the perimeter of the vault's upper slab (Figure 3d). Two steel profiles UPN 200 are located over the arch in the middle of the room. A complex steel confinement device composed of IPN 100 profiles is located at each corner, in addition to the horizontal steel profiles (Figure 3d, see also Figure 2e).

3 EXPERIMENTAL STUDIES

3.1 Material tests

Compression tests were carried out in the laboratory to measure the compressive strength of eight brick samples of $110 \times 100 \times 45 \text{ mm}^3$ obtained by cutting bricks from the Administration pavilion. The tests were carried out according to the method specified by the EN-772-1 (CEN 2000). The average compressive strength was 30.1 MPa. The tests were also utilised to measure the Young's modulus of the bricks, for which an average value of 8,000 MPa was obtained.

The compression strength of masonry was measured upon two series of composite specimens. The first series (series 1) was built using bricks extracted from the building in combination with a new mortar designed to reproduce the original one. The second series of specimens (series 2), having the same arrangement and dimensions of the specimens of series 1, was extracted from real masonry vaults of the Administration pavilion. Specifically, the specimens were obtained from two masonry vaults that were demolished in order to accommodate staircases required to fulfil the new accessibility and safety requirements. For that purpose, the specimens were taken from the central part of the vaults in order to minimise their curvature and its possible influence on the mechanical properties. The geometry of the specimens, corresponding to the actual texture of the masonry composing the vaults, is shown in Figure 4. Both series provided very similar masonry compressive strength values, amounting respectively to 7.90 MPa (with standard deviation of 1.3 MPa) and 7.28 MPa (with standard deviation of 1.49 MPa). Debonding (i.e. separation of thin tiles) was observed at a lower compression stress value of about 3.67 MPa (with standard deviation of 0.28 MPa). In spite of the debonding, it was possible to apply a significant increase of compressive loading until reaching the mentioned compressive strength values.

The masonry Young's modulus was measured by placing vertical displacement transducers between the control points indicated in Figure 4. An average masonry Young's modulus of 2,500 MPa was obtained, yielding a ratio to the compressive strength of about 340.

3.2 Dynamic identification

More than 95 dynamic tests were carried out on the masonry vaults of the Administration building of the Hospital de Sant Pau. Specifically, dynamic tests were carried out on the vaults A, B and C. Their results were systematically compared to the corresponding numerical results as a way to validate the FEM models.

The pattern used for the assessment of the masonry vaults system was based on a mesh consisting of 25 points radially distributed (Figure 5a). In four of these points (nodes 1, 5, 11 and 13) uniaxial accelerometers were located. Such a pattern was locally adjusted to the particular geometry of the different vaults. A minimum of 4 valid impacts were performed at each of the points of the mesh and their results subsequently averaged. Using the reciprocity principle, the matrix containing the frequency response functions (FRF) was filled out, and therefrom the modal model and its parameters deduced. The excitation was caused with an impact hammer with a mass of 5.50 kg. The vibration was measured by means of piezoelectric accelerometers with frequency range between 0.15 and 1,000 Hz. Figure 5b shows the positioning of the experimental set up in vault A. Figure 5c shows the accelerometer installed for measurements of vault A. This position corresponds to the point 1 reported in Figure 5a. Table 1 summarises the results obtained on the first three natural frequencies measured for vaults A, B and C.

3.3 Static loading test on vault B

A static loading test was carried out on one of vaults B in the Administration pavilion in September 2010. A loading/unloading procedure using water tanks (Figures 6a, b) was carried out on the entire slab involving the application of a maximum distributed load of 4.0 kN/m². The total duration of the test was 48 hours (Figure 6c). The maximum deflection obtained at points 1

and 2 were 1.2 mm and 1.5 mm, respectively (Figure 6d). No cracking on the vault was observed during the test.

4 NUMERICAL SIMULATION OF THE EXPERIMENTAL BEHAVIOUR

4.1 Description of the models

Vaults A, B and C of the Administration pavilion were studied by means of the FE method. The analyses were carried out considering material nonlinearity.

4.1.1 Mechanical parameters and constitutive laws

The compressive strength of masonry was estimated considering different empirical correlations (Eurocode 6 [CEN, 2005b] and PIET 70 [PIET 70, 1971]). The results from the tests mentioned in Section 3.1 were also taken into account. In spite of the value obtained experimentally (about 7 MPa), the adopted compressive strength for calculation purposes was limited to 4 MPa because of the limited experimental information and the expected scattering of the material properties in the building. The tensile strength was assumed as 5% of the compressive strength. This value was assumed taking into account the typical values presented in different national codes (PIET 70, 1971, Italian Ministry of Infrastructure and Transport, 2009). For the Young's modulus, a value of 2,000 MPa, similar to that determined experimentally, was adopted, considering also the aforementioned codes as a reference. For the tensile fracture energy, the adopted value was equal to 50 N/m. A density equal to 1,800 kg/m³ was considered. The Rankine's failure criterion in tension and the Drucker-Prager's failure criterion in compression were considered. A Coulomb friction model was assumed for the masonry-masonry contacts. This model was adopted for the description of the contact between the upper slab and the stiffening diaphragms at the extrados of the vault, and also between the diaphragms and the vault. Due to the lack of more specific evidence based on previous experiments, tentative frictional values were considered on the basis of previous experience to model such contacts. A friction angle of 36.9° (with $\tan\phi$ equal to 0.75) was adopted in combination with a cohesion of 0.2 MPa. The masonry-masonry contact was modelled with interface elements requiring as

input data values of the normal and shear linear stiffness. The values considered for such parameters were 100 MPa/mm and 50 MPa/mm, respectively.

The mechanical properties of steel were determined based on the information available on the documents of the time of the construction. The recommendations on steel mechanical properties for historical steelwork by the British constructional steelwork association were also taken into consideration (Bates 1984). The adopted yield stress both in tension and compression was 250 MPa. A density equal to 7,850 kg/m³ was considered. The Von Mises yield criterion was adopted.

4.1.2 FEM mesh

The prepared models describe the vault, exterior walls, slab, stiffening diaphragms at the extrados of the vault and steel profiles (Figure 7). The slab and diaphragms were modelled with a thickness of 0.10 m. The locations of the stiffening diaphragms are presented in Figures 7b, d, f. Taking advantage of the vaults' symmetry, only one-fourth of the vault was modelled, while adopting appropriate boundary conditions. The walls, slabs, vaults and diaphragms were modelled with curved 8-node quadrilateral and 6-node triangular elements. The steel profiles were modelled with 2-node straight beam elements. The masonry-masonry contact behaviour was modelled with 4-node line interface elements. The A, B and C vault model was respectively composed of 12,352, 18,828, 4,937 nodes and 13,320, 19,688, 5,582 elements (Figure 7). The model was restrained by rotationally fixed supports along the base of the walls.

4.2 FEM simulations

4.2.1 FEM simulation of vault A

Natural frequencies obtained from the experiment discussed in Section 3.2 are compared with those obtained from the FEM modal analysis for each kind of vault (A, B and C). Three models are compared. They are called model [a], model [b] and model [c], respectively. Model [a] is the same presented in Section 3.1. It is composed of the vault, walls, steel profiles, stiffening

diaphragms and slab. Model [b] is obtained by removing the slab from model [a]. Model [c] is the result of removing the slab and diaphragms from model [a]. For model [b] and model [c], the weight of the removed structural elements (slab and diaphragms) is taken into account so that the three models possess the same total weight.

The three alternative models provide natural frequencies close to those measured experimentally in the real structure (Table 2), showing that the influence of the secondary structural members on the dynamic response (at least, on the natural frequencies) is limited. For the three alternative models, the first vibration mode shows a mass participation factor equal to about 14.0% of the total mass in the translational x and y direction. This mode shows deformation in the walls (Figure 8).

4.2.2 FEM simulation of vault B

Also for vault B, the natural frequencies obtained from the experiment discussed in Section 3.2 are compared with those resulting from FEM modal analysis.

The influence of the secondary structural members on the dynamic response is more noticeable than for vault A. Model [a] shows good agreement with the real structure for the three vibration modes considered (Table 3). In turn, model [b] and model [c] show slightly lower natural frequencies than the real structure. The mass participation factor of the first vibration mode for the three models (models [a], [b], and [c]) is 13.5%, 12.4%, 15.0% in the translational y direction. This mode involves deformation mainly in the wall along the x direction (Figure 9). Unlike the vault A model, noticeable mass participation is seen only in the y direction. This is presumably due to the different shape of the vault in plan. In the vault B model, the wall along the x direction (6.7 m) is longer span than that along the y direction (6.2 m) while the vault A model is square in plan ($3.12 \times 3.12 \text{ m}^2$).

Using the same three models, the static loading test discussed in Section 3.3 was simulated. The deflection-loading relation at the centre and 1/4 of the span of the vault is presented in Figure 10a. For the observed locations, model [a] shows a similar stiffness to that of the real structure both in the loading and the unloading processes. However, when the slab and diaphragms are not included in the model (e.g. model [b] and model [c]), the stiffness becomes lower than that observed in the real structure (Figure 10b). The three models show no damage after applying the load, in agreement with the in-situ experiment. It is added that the three models did not show sliding through the masonry-masonry contacts during the simulation.

Using the model [a], the capacity of vault B under a uniform load was assessed by simulating and increasing load process up to failure. During the simulated loading process, damage starts to appear in the connections between the slab and the walls for an applied load of 10.7 kN/m². Sliding of the slab occurs at his load. Damage in the vault is observed at a load of 12.8 kN/m². The obtained maximum load capacity is 16.6 kN/m² and the corresponding deflection at the centre of the vault is 13.9 mm (Figure 11a). At this load, damage is visible in both extrados and intrados of the vault (Figure 11c-d). Evident damage is observed in the connections between the slab and the walls (Figure 11b).

A second analysis on the model [a] a was carried out with applied safety factors over the dead load (1.35) and over the live load (1.5) presented in Eurocode 0 (CEN 2005a) and also with reduced values of the material properties (with factors of 2.5 and 1.15 applied respectively over masonry and steel [CEN 2005b]) in order to study the maximum loading capacity obtained when conventional safety criteria are considered. The resulting maximum acceptable live load is assessed equal to 6.67 kN/m².

Using model b and model [c], the influence of the secondary structural members (upper slab and extrados stiffening diaphragms) over the capacity of the vault was analysed. As expected, the removal of these structural elements causes a decrease of both the load capacity and the

stiffness (Figure 11a). The obtained maximum load for model [b] is 13.6 kN/m². At the observed maximum load, the model b shows damage initiated at the connection between the vault and walls (Figure 12a, b). The obtained maximum load for model [c] is 8.22 kN/m². At the observed maximum load, the model [c] also shows damage propagating from the connection between vault and walls (Figure 12c, d). Therefore, the analysis predicts that the removal of the upper slab would decrease the capacity by 18.1% while the removal of the stiffening diaphragms and slab would decrease the capacity by 39.6%. This study shows that both the slab and the extrados diaphragms have a remarkable influence on the strength of the vault. It is important to mention, however, that the analysis carried out has a tentative value due to the lack of specific information due to the difficulty in characterising the mechanical and frictional properties of the connection between the vault and its secondary elements.

4.2.3 FEM simulation of vault C

Natural frequencies obtained from the above-discussed experiment (Section 3.2) are compared with those from FEM modal analysis. For the three modes shown in Table 4, model [a] shows slightly higher natural frequencies than the real structure. On the other hand, model [b] and model [c] show natural frequencies lower than those measured in the real structure, especially for the first mode. The first mode shows a participation factor equal to 5.8%, 4.4%, 3.2% respectively for model [a], model [b] and model [c] in the z direction (vertical). In the vault C model, the deformation is concentrated in the vault while in the vault A, B models the deformation was seen in the walls (Figure 13, see, Figure 8, 9). This difference is supposed to be derived from longer span of the vault than in the other two vault models.

5 DISCUSSION

The present study has included an investigation on the role and the influence of the secondary elements of timber vaults on their load capacity and stiffness. Such secondary elements include the upper horizontal slab and the extrados diaphragms supporting the slab. The influence of these elements has been analysed for different vaults representing different span ranges. As

expected, the influence of these elements over the load capacity and stiffness is more important for longer vault spans.

In particular, it has been necessary to include such secondary elements in the numerical model in order to obtain a satisfactory agreement with the stiffness measured during the execution of a static load test in vault B (vault with intermediate span). The explicit modelling of these elements has provided a satisfactory numerical prediction of the frequencies corresponding to the first three vibration modes measured experimentally. It must be remarked that the analysis have been carried out by adopting a value for the Young's modulus of masonry close to that measured experimentally.

In the studied FEM model, the masonry-masonry contacts between slab and diaphragms and also between diaphragms and vault have been modelled by means of a Mohr-Coulomb friction model. For tentative frictional values of the masonry-masonry contacts, the analysis suggests that the bonding between the different masonry elements is active up to a significant load level. Specifically, the comparison with the static load test carried out for vault B (spanning 6.7 m) indicates that no sliding at the masonry-masonry contacts occurs for the maximum loads applied during the experiment (4 kN/m^2) and beyond. The simulation of a loading process up to failure, for this vault, suggests that sliding would occur for a load of 10.7 kN/m^2 , representing 65% of the ultimate load predicted. Removing the secondary structural elements from the model induces very significant reductions of the load capacity and stiffness. In the case of vault B, the removal of the slab causes a reduction of the load capacity of 19%, while the removal of both the slab and stiffening diaphragms causes a reduction of 51%.

The comparison of the numerical predictions with the experimental reference values has allowed a partial validation of the numerical models. The models could be used, in a further step, to carry out a load capacity assessment of the vaults of the buildings analysed. However, and before carrying out an accurate assessment, further experimental investigation would be

convenient for a more accurate characterisation of the material properties and, specifically, of the frictional parameters in the masonry-masonry contacts.

6 CONCLUSIONS

A study on a set of real timber vaults has been presented in which experimental and numerical techniques have been combined and integrated in order to conclude on their static and dynamic performance. The investigated vaults are located in the Administration pavilion of the Hospital de Sant Pau of Barcelona. The study has combined experiments on masonry samples, oriented to determine the strength and deformability parameters in compression of the timber vault's masonry, with in-situ experiments and numerical simulation. The tests carried out over the real vaults (static loading test and dynamic tests) have contributed to better understand the structural response of the vaults.

The numerical models have satisfactorily predicted the experimental response obtained in the static and dynamic tests, confirming the adequacy of the numerical approach utilised, based on a continuous non-linear FEM description, for the analysis of this type of structural elements.

As shown by the analyses, secondary construction members, such as the upper slab and the stiffening diaphragms sustaining the slab, can contribute significantly to the stiffness and strength of timber vaults, especially for long spans. In some of the cases studied, the inclusion of such secondary elements has been necessary in order to obtain a satisfactory simulation of the experimental response.

In the present research, frictional behaviour has been taken into consideration at the masonry-to-masonry contacts between the diaphragms and horizontal structural elements (the upper slab and vault). In addition to a more realistic description, it has reduced the likelihood of possible numerical problems. However, it has to be added that a more detailed characterisation of the frictional behaviour of this type of contact would require specific experimental investigation.

ACKNOWLEDGMENTS

The authors gratefully acknowledge the financial support from the MINECO (Ministerio de Economía y Competitividad of the Spanish Government) and the ERDF (European Regional Development Fund) through the MULTIMAS project (Multiscale techniques for the experimental and numerical analysis of the reliability of masonry structures, ref. num. BIA2015-63882-P).

REFERENCES

- Araguas, P. 1999. Voute a la rousillon. Butlletí de la Reial Acadèmia Catalana de Belles Arts Sant Jordi 13: 173-185.
- Bates, W. 1984. Historical structural steelwork handbook. Westminster: The British Constructural Steelwork Association.
- Casals, A., González, J. L., Onecha, B., Sanmartí, C. 2011. Las razones del uso masivo de la bóveda tabicada en el Hospital de Sant Pau de Barcelona: una hipótesis para el debate. Simposio Internacional sobre Bóvedas Tabicadas. Valencia, 2011.
- CEN. 2005a. EN 1990+A1: Eurocode – Basis of structural design. Brussels: Comité Européen de Normalisation.
- CEN. 2005b. EN 1996-1-1: Eurocode 6: Design of Masonry Structures – Part 1-1: Common Rules for Reinforced and Unreinforced Masonry Structures. Brussels: Comité Européen de Normalisation.
- Collins, G. R. 1968. The Transfer of Thin Masonry Vaulting from Spain to America. Journal of the Society of Architectural Historians 27(3): 176-201.
- De Llorens, D. J. I. 2013. Wine cathedrals: making the most of masonry. Proceedings of the ICE-Construction Materials, 166(6), 329-342.
- D’Espie, C. F. F. 1754. Maniere de rendre toutes sortes d’édifices incombustibles. Paris: Duchesne.
- European Committee of Standardization (CEN). 2000. EN 772 1:2011 Methods of Test for Masonry Units. Part 1: Determination of the Compressive Strength. Brussels: Comité Européen de Normalisation.
- Ferrario, L., Marini, A., Andreis, V., Zanotti, S., Riva, P., Giuriani, E. 2012. Behaviour and retrofitting of simple-leaf vaults under distributed horizontal forces. Proceedings of the SAHC 2012 Conference, Wrocław, 1503-1511.
- Fray Lorenzo de San Nicolás. 1796. Arte y Uso de Arquitectura. Retrieved from

<https://archive.org/details/arteyusodearquit02lore>

- González, J. L. 1999. La bóveda tabicada. Su historia y su futuro. Teoría e historia de la rehabilitación. Teoría e historia de la restauración 1: 237-259.
- González, J. L. 2005. La bóveda tabicada: entre la conservación y la destrucción. Informes de la Construcción 56(496): 67-72.
- González, J. L., Casals, A., Sanmarti, C., Onecha, B. 2011. Los sistemas de estribado de las bóvedas tabicadas del hospital de Sant Pau Barcelona: tirantes, zunchos y pórticos. Actas del Séptimo Congreso Nacional de Historia de la Construcción: 583-592.
- Guastavino, R. 1893. Essay on the theory and history of cohesion system. Boston: Ticknor and company.
- Gulli, R., Mochi, G. 1995. Bovedas tabicadas: Architeaura e cosruzione. Rome: COI' Editrice.
- Huerta, S., López, M. G., Redondo, M. E. 2001. Bibliografía seleccionada y comentada sobre Guastavino y la construcción tabicada. In Las bóvedas de Guastavino en América. S. Huerta (ed.). Madrid: Instituto Juan de Herrera, CEHOPU: 373-393.
- Huerta, S. 2003. The Mechanics of timbrel vaults: A Historical Outline. Essays on the History of Mechanics Berlin, Germany: Birkhauser Verlag: 89-134.
- Italian Ministry of Infrastructure and Transport. 2009. Circolare 2 febbraio 2009, n. 617 Istruzioni per l'applicazione delle «Nuove norme tecniche per le costruzioni» di cui al decreto ministeriale 14 gennaio 2008
- López, L. D., Domènech, R. M., Palumbo, F. M. 2014. "Brick-topia", the thin-tile vaulted pavilion. Case Studies in Structural Engineering 2, 33-40.
- Moya, L. B. 1947. Bóvedas tabicadas. Madrid: Ministerio de Fomento, Centro de Publicaciones.
- Palizzolo, L., Benfratello, S., Caffarelli, A., Giambanco, F., Urso, R. 2008. Bòvedas tabicadas: experimental and numerical analysis. High Performance Structures and Materials IV 97: 503-512.
- PIET 70. 1971. Prescripciones técnicas del Instituto Torroja. Madrid: Technical requirements from the Torroja Institute.
- Redondo, M. E. 2012. Test on Tile Vaults in France in the 19th Century. Fourth International Congress on Construction History, Paris, 2012:107-115.
- Truño, Á. 2004. Construcción de bóvedas tabicadas. Madrid: Instituto Juan de Herrera Escuela Técnica Superior de Arquitectura.

LIST OF FIGURE CAPTIONS

Figure 1 - Original drawing showing the general plan and distribution of the pavilions of the Hospital de Sant Pau as envisaged by Domènech i Montaner.

Figure 2 - Administration pavilion of the Hospital de Sant Pau: (a) façade, (b) vault decorated with tiles, (c) plan, (d) 3D view and (e) basement floor of west middle and extreme body (d-e from González et al. 2011)

Figure 3 - Administration pavilion: (a) vault A, (b) vault B, (c) vault C and (d) sketch of the steel confinement structure located at the corners of vault C.

Figure 4 - Geometry of the masonry specimens tested in compression with the distribution of the measurement points.

Figure 5 - In-situ dynamic identification test. : (a) location of the accelerometers in the tested vaults, (b) measurement positioning of the experimental set up placed in a in vault A and (c) accelerometer installed in a used for measurements of vault A..

Figure 6 - Vault B, Administration pavilion: (a) water tanks on the slab, (b) location of accelerometers (c) loading/unloading process and (d) load-deflection curves measured at points 1 and 2.

Figure 7 - FEM model of vaults in the Administration pavilion; (a), (b): model of vault A; (c), (d): model of vault B; and (e), (f): model of vault C.

Figure 8 - The first mode shape, vault A: (a) model [a], (b) model [b] and (c) model [c].

Figure 9 - The first mode shape, vault B: (a) model [a], (b) model [b] and (c) model [c].

Figure 10 - Comparisons between experimental and FEM load-deflection curves for vault B: (a) model a at points 1-2, (b) models a, b, c at point 1.

Figure 11 - Application to vault B model of an incremental uniform load: (a) load-deflection curve at the centre of the vault and principal strain contours close to the ultimate condition for the entire model (b), vault extrados (c) and vault intrados (d).

Figure 12 - Principal strain distribution close to the ultimate condition for model [b] and model [c]. Entire model [b] (a), intrados of model [b] vault (b), entire model (c), and intrados of model [c] vault (d).

Figure 13 - The first mode shape, vault C: (a) model [a], (b) model [b] and (c) model [c].

LIST OF TABLE CAPTIONS

Table 1 - Natural frequencies from the on-site dynamic experiments.

Table 2 - Comparison of the natural frequencies observed from the dynamic experiment and the FEM analyses, vault A

Table 3 - Comparison of natural frequencies observed from the dynamic experiment and the FEM analyses, vault B.

Table 4 - Comparison of natural frequencies observed from the dynamic experiment and FEM analyses, vault C.

Figures

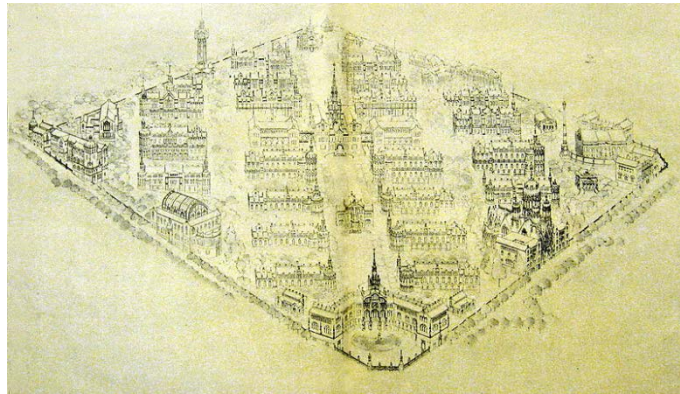


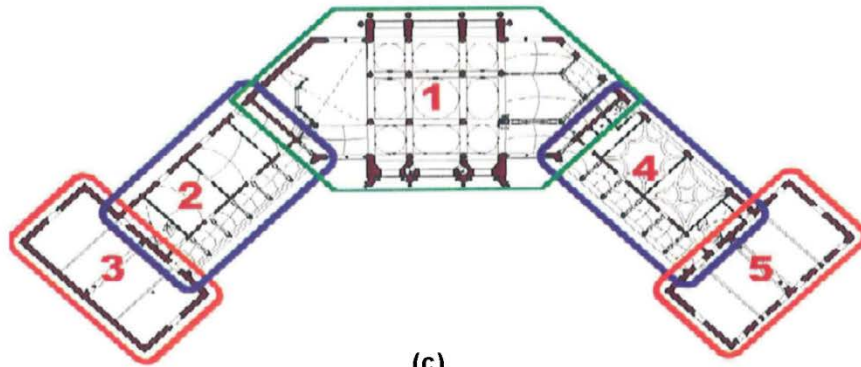
Figure 1 - Original drawing showing the general plan and distribution of the pavilions of the Hospital de Sant Pau as envisaged by Domènech i Montaner.



(a)



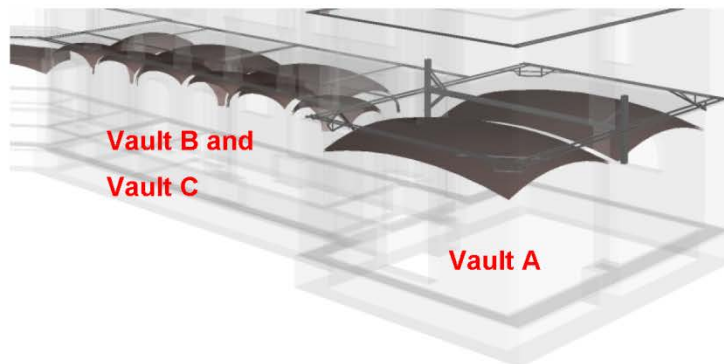
(b)



(c)



(d)



(e)

Figure 2 - Administration pavilion of the Hospital de Sant Pau: (a) façade, (b) vault decorated with tiles, (c) plan, (d) 3D view and (e) basement floor of west middle and extreme body (d-e from González et al. [2011])



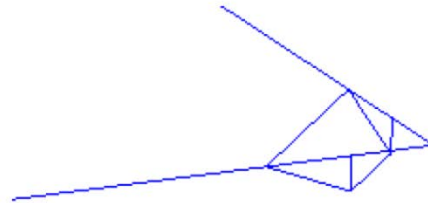
(a)



(b)



(c)



(d)

Figure 3 - Administration pavilion: (a) vault A, (b) vault B, (c) vault C and (d) sketch of the steel confinement structure located at the corners of vault C.

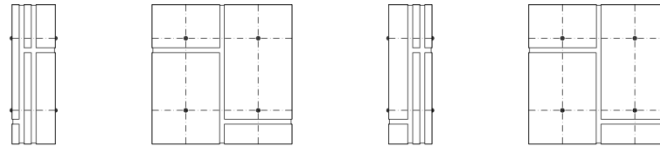
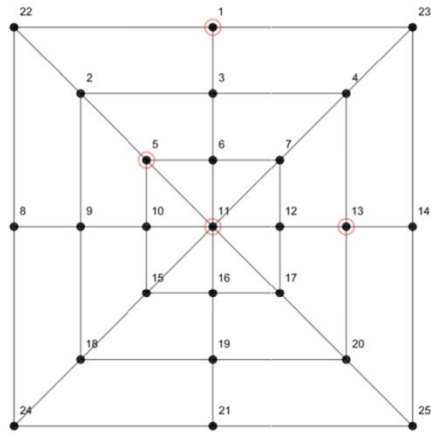


Figure 4 - Geometry of the masonry specimens tested in compression with the distribution of the measurement points.



(a)



(b)

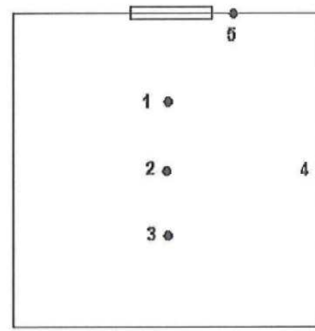


(c)

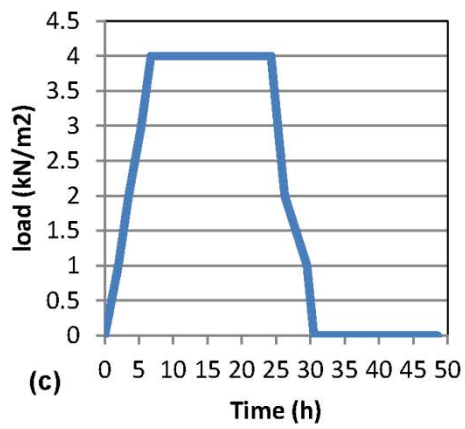
Figure 5 - In-situ dynamic identification test: (a) location of the accelerometers in the tested vaults, (b) positioning of the experimental set up in vault A and (c) accelerometer used for measurements of vault A.



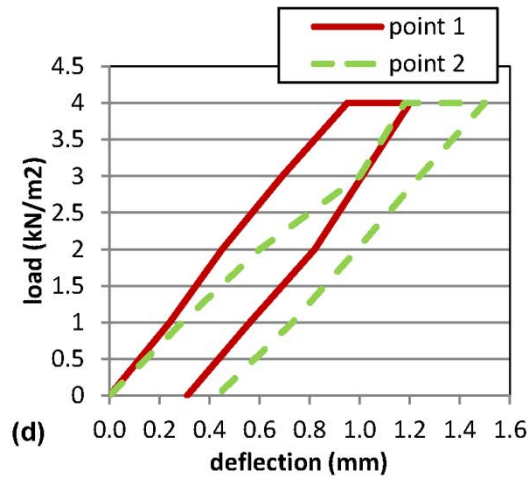
(a)



(b)



(c)



(d)

Figure 6 - Vault B, Administration pavilion: (a) water tanks on the slab, (b) location of accelerometers (c) loading/unloading process and (d) load-deflection curves measured at points 1 and 2.

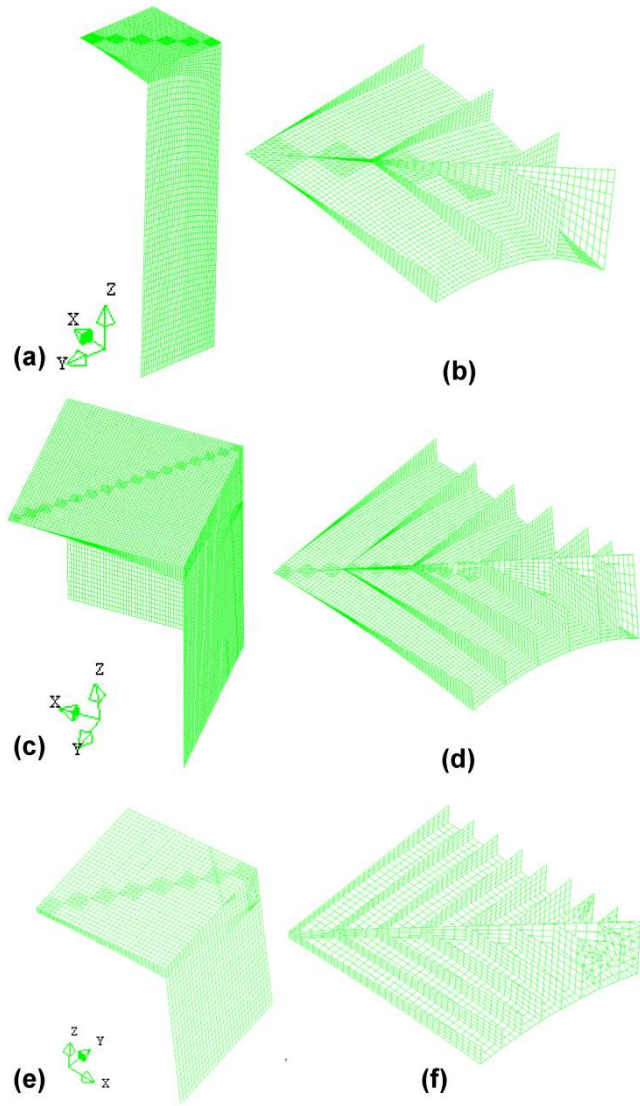


Figure 7 - FEM model of vaults in the Administration pavilion; (a), (b): model of vault A; (c) ,(d): model of vault B; and (e), (f): model of vault C.

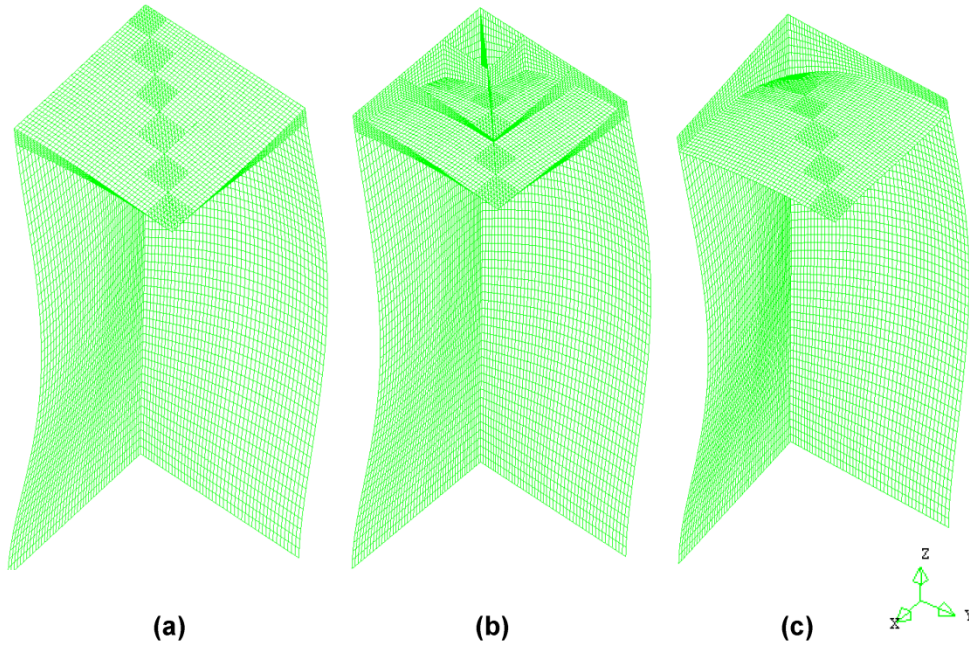


Figure 8 - The first mode shape, vault A: (a) model a, (b) model b and (c) model c.

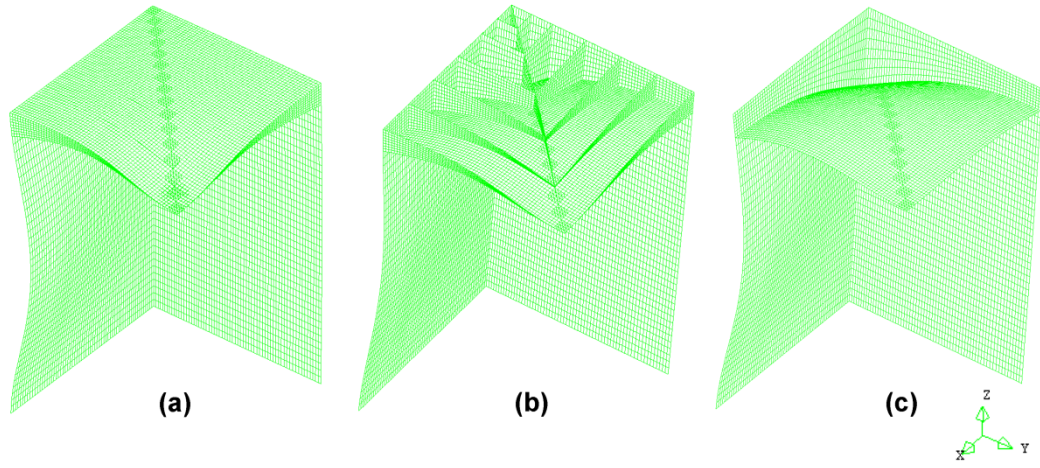
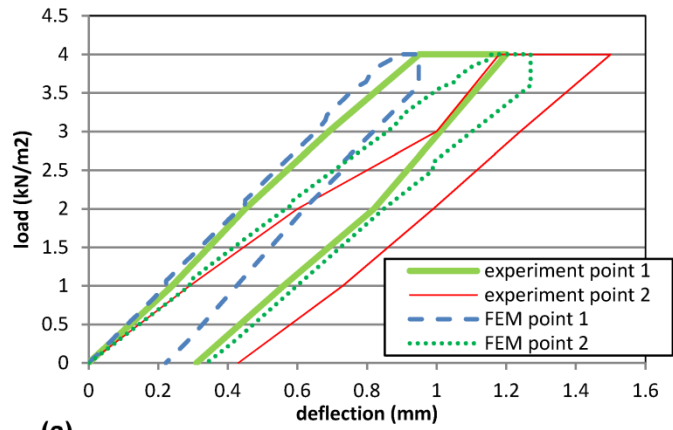
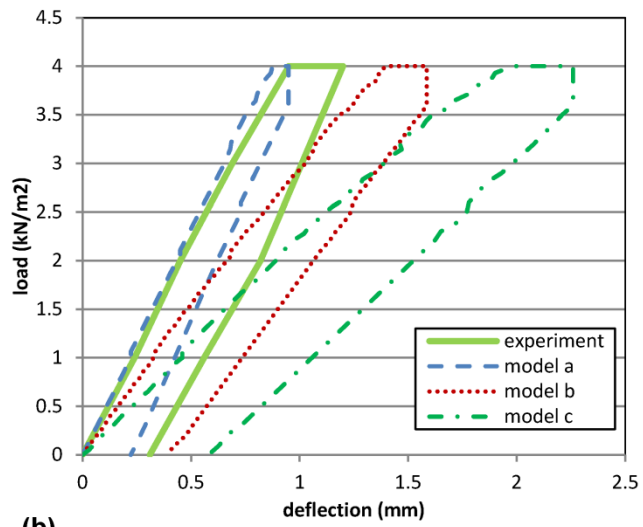


Figure 9 - The first mode shape, vault B: (a) model a, (b) model b and (c) model c.



(a)



(b)

Figure 10 - Comparisons between experimental and FEM load-deflection curves for vault B: (a) model a at points 1-2, (b) models a, b, c at point 1.

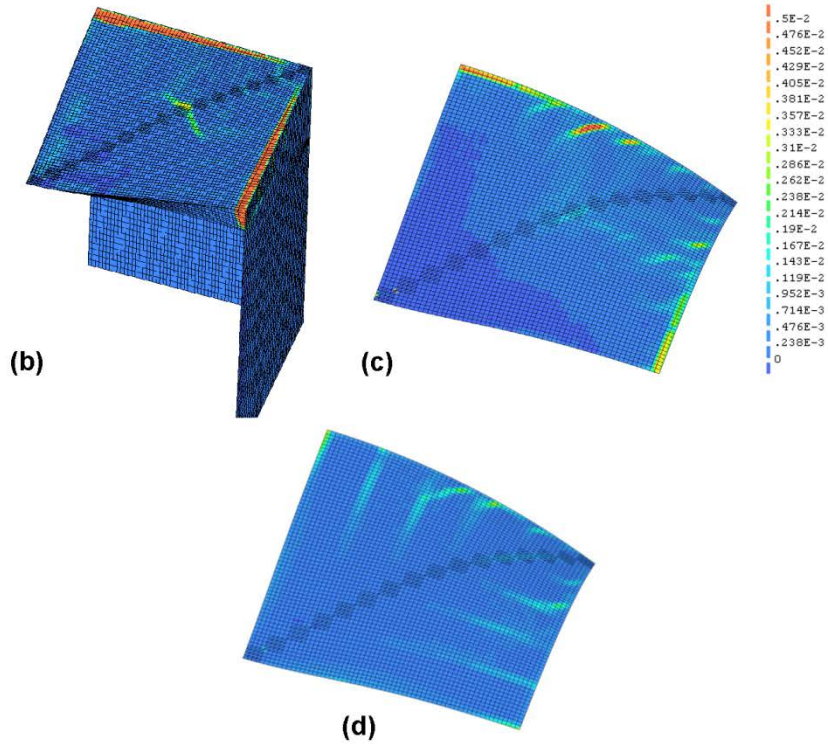
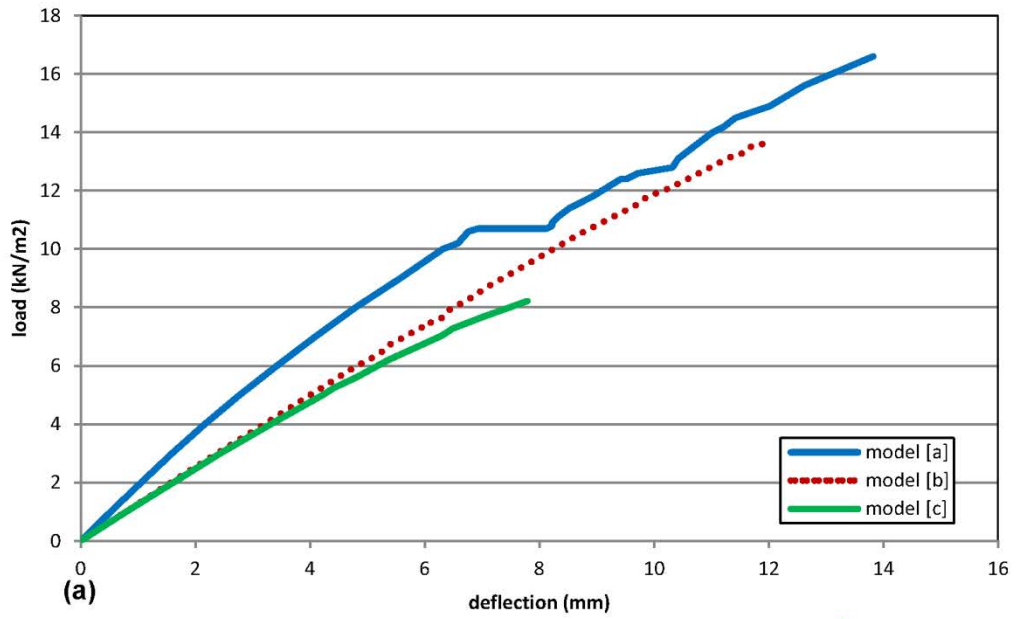


Figure 11 - Application to vault B model of an incremental uniform load: (a) load-deflection curve at the centre of the vault and principal strain contours close to the ultimate condition for the entire model (b), vault extrados (c) and vault intrados (d).

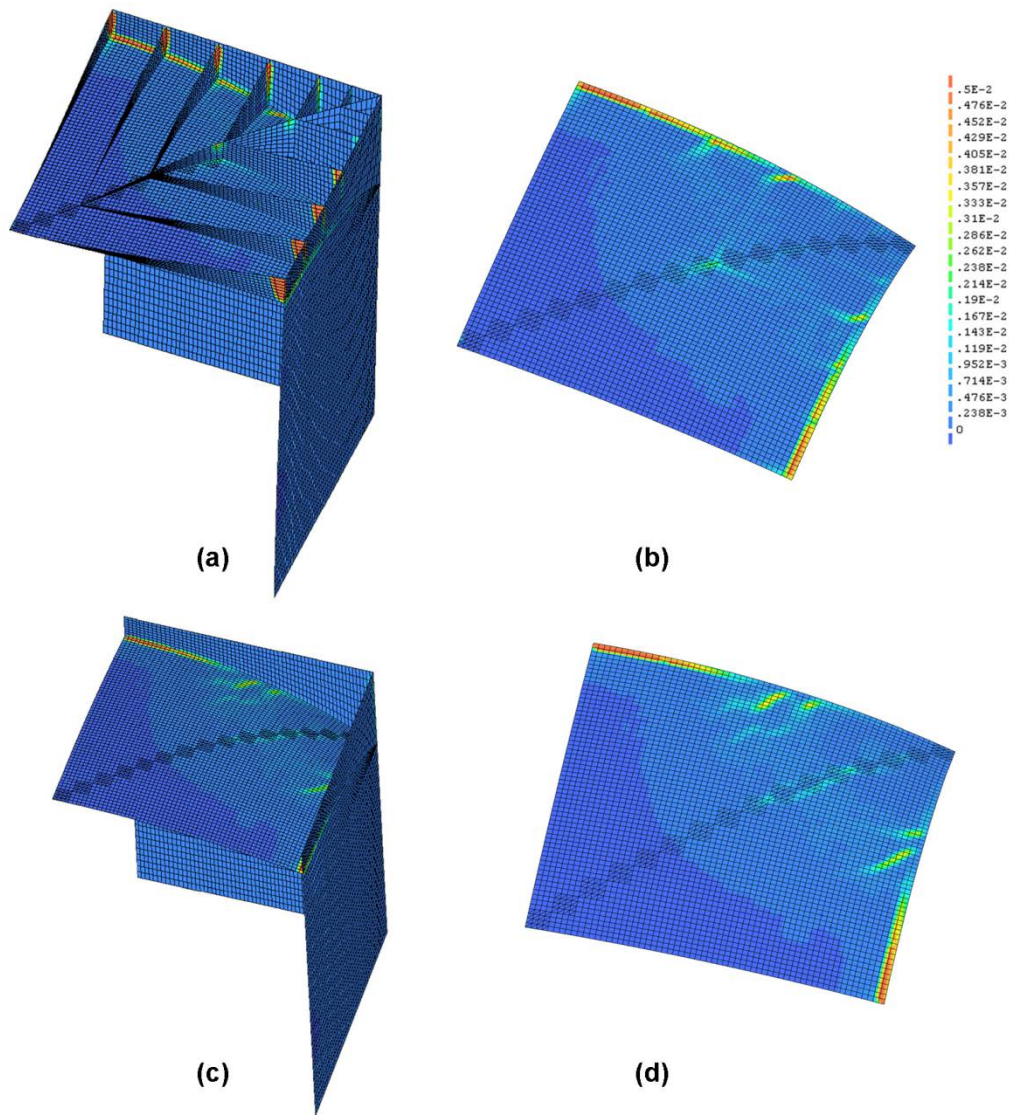


Figure 12 - Principal strain distribution close to the ultimate condition for model b and model c. Entire model b (a), intrados of model b vault (b), entire model (c), and intrados of model c vault (d).

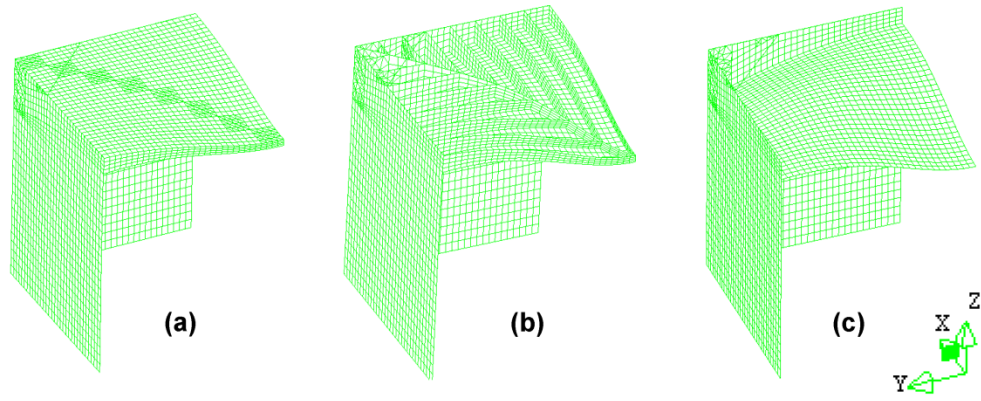


Figure 13 - The first mode shape, vault C: (a) model a, (b) model b and (c) model c.

Table 1 - Natural frequencies from the dynamic experiments.

(Hz)	1st	2nd	3rd
Vault A	22.67	39.79	47.97
Vault B	16.99	24.24	38.80
Vault C	9.79	21.93	23.39

Table 2 - Comparison of the natural frequencies observed from the dynamic experiment and the FEM analyses, vault A

Hz	1st	2nd	3rd
Experiment	22.67	39.79	47.97
Model a	24.49	40.02	47.18
Model b	24.27	39.82	47.56
Model c	24.18	39.56	47.97

Table 3 - Comparison of natural frequencies observed from the dynamic experiment and the FEM analyses, vault B.

Hz	1st	2nd	3rd
Experiment	16.99	24.24	38.80
Model a	16.86	24.08	38.53
Model b	16.27	23.52	36.36
Model c	15.75	22.15	34.20

Table 4 – Comparison of natural frequencies observed from the dynamic experiment and FEM analyses, vault C.

Hz	1st	2nd	3rd
Experiment	9.79	21.93	23.39
Model a	10.20	23.34	24.60
Model b	5.97	17.71	22.36
Model c	2.93	15.30	21.21